

Inverse Optimal Control with Incomplete Observations

Wanxin Jin¹, Dana Kulić², Shaoshuai Mou¹ and Sandra Hirche³

Abstract—In this article, we consider the inverse optimal control problem given incomplete observations of an optimal trajectory. We hypothesize that the cost function is constructed as a weighted sum of relevant features (or basis functions). We handle the problem by proposing the recovery matrix, which establishes a relationship between available observations of the trajectory and weights of given candidate features. The rank of the recovery matrix indicates whether a subset of relevant features can be found among the candidate features and the corresponding weights can be recovered. Additional observations tend to increase the rank of the recovery matrix, thus enabling cost function recovery. We also show that the recovery matrix can be computed iteratively. Based on the recovery matrix, a methodology for using incomplete observations of the trajectory to recover the weights of specified features is established, and an efficient algorithm for recovering the feature weights by finding the minimal required observations is developed. We apply the proposed algorithm to learning the cost function of a simulated robot manipulator conducting free-space motions. The results demonstrate the stable, accurate and robust performance of the proposed approach compared to state of the art techniques.

Index Terms—Inverse optimal control, inverse reinforcement learning, incomplete trajectory observations

I. INTRODUCTION

Inverse optimal control (IOC), also known as inverse reinforcement learning (IRL), addresses the problem of inferring a reward function that explains observed system behaviors of the corresponding optimal control policy (Ng and Russell, 2000). Based on IOC, observations of expert demonstrations can be succinctly characterized and transferred to robots and other mechanisms (Abbeel et al., 2010; Kolter et al., 2008). Successful applications are broad, such as apprenticeship learning (Calinon et al., 2010; Zucker et al., 2011), humanoid robot control (Krstic and Tsiotras, 1999), autonomous driving (Kuderer et al., 2015), human-robot cooperation (Mainprice et al., 2015, 2016), etc.

The most common method in IOC is to formulate the cost function of observed trajectories as a linear combination of relevant features (or basis functions) with unknown weights (Abbeel and Ng, 2004; Ratliff et al., 2006; Ziebart et al., 2008). While varying techniques have been developed to recover the feature weights from complete observations of trajectories, utilizing incomplete observations for the recovery has been rarely explored. An approach capable of recovering cost functions from incomplete observations will be beneficial for three reasons: first, complete observations of the trajectory may not be available; second, computational cost of utilizing

existing IOC methods considering complete trajectories may be large; and third, IOC from incomplete observations may be useful for online identification of cost functions.

This article considers the inverse optimal control problem where we are given incomplete observations of an optimal trajectory. We establish a methodology for using incomplete observations of the trajectory to recover the weights of given candidate features.

The key idea is based on the *Recovery Matrix*, which establishes a relationship between available observations of the optimal trajectory, in terms of a set of candidate features, and the corresponding feature weights to be recovered. The matrix, together with its properties, provides the following insights for handling general IOC problems: (i) the rank of the recovery matrix indicates whether the feature weights can be recovered; (ii) additional observations tend to increase the rank of the recovery matrix, thus contributing to enabling recovery; (iii) the features that are irrelevant to express the optimal trajectory do not influence the recovery and can be identified; (iv) incomplete observations of the trajectory can suffice for inferring the feature weights; and (v) the IOC computation can be performed in an iterative and efficient fashion.

Based on the recovery matrix, we establish a methodology for using incomplete observations of an optimal trajectory to recover the weights of specified features, and then devise an efficient implementation to recover the feature weights by finding minimal observations of the trajectory.

We also demonstrate that the proposed recovery matrix can be employed to provide performance guarantees for cost function recovery (Molloy et al., 2018), handle trajectories of the local optimality (Levine and Koltun, 2012), and develop IOC techniques for infinite horizon problems. We show that recovery of the cost function based on complete trajectory observations by using existing techniques is a special case of our methodology.

A. Related Work

Existing IOC techniques can be categorized by whether the forward optimal control problems are computed within the procedure. One type is a nested iterative process involving an inner loop, where predicted trajectories of the corresponding forward problem are computed for a given cost function, and an outer loop, where the cost function (feature weights) is updated. This structure was initially utilized in (Abbeel and Ng, 2004) for learning unknown reward functions of a statistic Markov decision process, where IOC is more often referred to as inverse reinforcement learning. In their work, a criterion for recovering the feature weights is to maximize the margin between costs of the predicted and observed trajectories. A similar idea also appears in (Ratliff et al., 2006). Another

¹Wanxin Jin and Shaoshuai Mou are with the School of Aeronautics and Astronautics, Purdue University, Indiana, USA.

²Dana Kulić is with the Department of Electrical Computer Engineering, University of Waterloo, Waterloo, Canada.

³Sandra Hirche is with the Chair of Information-oriented Control, Technical University of Munich, Munich, Germany.

popular principle for updating cost functions (in the outer loop) is proposed in (Ziebart et al., 2008), by finding the feature weights such that the probability distribution over trajectories maximizes the entropy and simultaneously matches the feature values of observations. This maximum entropy IRL is then extended and applied to various scenarios, such as learning humanoid locomotion (Park and Levine, 2013), autonomous vehicles (Kuderer et al., 2015), and robot navigation (Vasquez et al., 2014). In (Mombaur et al., 2010), cost functions are obtained based on penalizing the deviations of the predicted trajectory from observed paths; similar methods are applied to studying human walking (Clever et al., 2016) and arm motion planning (Berret et al., 2011).

The nested algorithms have to solve the forward optimal control problem repeatedly, making cost function learning computationally costly. This motivates developing ways of directly recovering feature weights. The fundamental idea is based on constructing a set of optimality equations which hold for the observed optimal trajectories. The idea was first presented in (Keshavarz et al., 2011), where the Karush-Kuhn-Tucker (KKT) optimality conditions are used and the objective functions are solved by minimizing a residual to quantify violations of those conditions. (Puydupin-Jamin et al., 2012) applied the KKT-based method to IOC problems for analysis of human locomotion. Other successful works include (Johnson et al., 2013) where a residual optimization is established based on the Pontryagin’s Minimum principle, (Aghasadeghi and Bretl, 2014) where the Euler Lagrange equations in continuous cases are employed, and (Dvijotham and Todorov, 2010), where the Hamilton-Jacobi-Bellman equations are used.

Recently, direct IOC methods have been applied to more complex tasks. For example, a framework of inverse KKT is proposed in (Englert et al., 2017) to recover cost functions during object manipulation. Another interest of direct IOC methods is to explore the ‘recoverability’ of IOC problems given demonstrations. For example, when a system motion remains at equilibrium point, the trajectory, though satisfying optimality equations, is uninformative to help with inferring the cost function. This issue is addressed in (Molloy et al., 2016, 2018), where a sufficient condition for feature weights recovery is presented given complete trajectory observations.

To the best of our knowledge, existing IOC approaches are based on complete observations of the optimal trajectory, and IOC under incomplete observations is rarely investigated. We consider the IOC problem with incomplete observations due to the following motivations. First, complete observations of system trajectories may not be available in practice. Second, though direct IOC methods achieve improved computational efficiency compared to nested ones, the computational cost is still significant especially when handling action spaces of high dimensionality. Third, utilizing incomplete observations benefits other applications such as motion segmentation and behavior identification, where the underlying cost functions may be varying (Lin et al., 2016).

B. Contributions

In this article, we solve the IOC problem with incomplete trajectory observations through analysis of the *recovery matrix*. The recovery matrix is defined based on the available observations of the optimal trajectory and a candidate feature set. We show that recovery of the weights corresponding to the candidate features is related to the recovery matrix by its rank and kernel. We present some properties associated with the recovery matrix, which provides insights for handling IOC in terms of trajectory observations and feature set selection. We also present an iterative formula to efficiently compute the recovery matrix. Based on the recovery matrix, we establish a method for using incomplete observations of the optimal trajectory to recover the weights of specified features. Furthermore, we develop an efficient algorithm for recovering the weights from minimal observations of the trajectory.

The article structure is as follows. The IOC problem is formulated in Section II. In Section III, we propose the recovery matrix and present its properties as well as implementation. In Section IV, we develop the methodology and algorithm for IOC with incomplete observations. The proposed approach is evaluated in Section V and conclusions are in Section VI.

C. Notation

- The column operator $\text{col} \{ \mathbf{x}_1, \mathbf{x}_2, \dots, \mathbf{x}_k \}$ stacks its vector arguments into a column (concatenation vector).
- $\mathbf{x}_{(k:k+n)}$ denotes a stack of multiple vectors from time k to $k+n$, that is, $\mathbf{x}_{(k:k+n)} = \text{col} \{ \mathbf{x}_k, \mathbf{x}_{k+1}, \dots, \mathbf{x}_{k+n} \}$.
- \mathbf{A} (bold-type) denotes a block matrix.
- Given any function $\mathbf{f}(\mathbf{x})$ and a constant \mathbf{x}^* , $\frac{\partial \mathbf{f}}{\partial \mathbf{x}^*}$ denotes the Jacobian matrix with respect to \mathbf{x} evaluated at \mathbf{x}^* .
- Zero matrix or vector is denoted as $\mathbf{0}$, and identity matrix is denoted as I , both with appropriate dimensions.
- $\sigma_i(\mathbf{A})$ denotes the i th smallest singular value of matrix \mathbf{A} ; e.g. $\sigma_1(\mathbf{A})$ is the smallest singular value.
- $\ker \mathbf{A}$ denotes the kernel of matrix \mathbf{A} .

II. PROBLEM FORMULATION

Consider the following discrete-time system¹

$$\mathbf{x}_{k+1} = \mathbf{f}(\mathbf{x}_k, \mathbf{u}_{k+1}), \quad \mathbf{x}_0 \in \mathbb{R}^n, \quad (1)$$

where $\mathbf{f}(\cdot, \cdot) : \mathbb{R}^n \times \mathbb{R}^m \mapsto \mathbb{R}^n$ is differentiable; $\mathbf{x}_k \in \mathbb{R}^n$ denotes the state; $\mathbf{u}_k \in \mathbb{R}^m$ is the control input; and k is the time index. Suppose that an optimal trajectory of states and inputs $(\mathbf{x}_{1:T}^*, \mathbf{u}_{1:T}^*)$ (locally) minimizes the cost function

$$J(\mathbf{x}_{1:T}, \mathbf{u}_{1:T}) = \sum_{k=1}^T \omega^* \phi^*(\mathbf{x}_k, \mathbf{u}_k), \quad (2)$$

where $\phi^* : \mathbb{R}^n \times \mathbb{R}^m \mapsto \mathbb{R}^s$ is called a *relevant feature vector* and is defined as the column of a *relevant feature set*

$$\mathcal{F}^* = \{ \phi_1^*, \phi_2^*, \dots, \phi_s^* \}, \quad (3)$$

¹In (1), at time k , we denote the control input as \mathbf{u}_{k+1} instead of \mathbf{u}_k for notation simplicity of following descriptions, as used in (Zucker et al., 2011).

that is, $\phi^* = \text{col } \mathcal{F}^*$, with the i th entry ϕ_i^* representing a relevant feature for the running cost, and $\omega^* \in \mathbb{R}^s$ is called the weight vector, with the i th entry ω_i^* called the feature weight corresponding to ϕ_i^* . This type of weighted-feature cost function is typically used for IOC problems (Abbeel and Ng, 2004; Molloy et al., 2018; Ziebart et al., 2008), and successfully employed in a wide range of applications (Englert et al., 2017; Kuderer et al., 2015; Lin et al., 2016).

The goal of IOC is to recover the cost function by finding a relevant feature set \mathcal{F}^* and recovering the corresponding weight vector ω^* . Note that the weight vector for the given relevant feature vector can only be determined up to a non-zero scaling factor (Molloy et al., 2018), because $c\omega^*$ with $c > 0$ can lead to the same trajectory as by ω^* . Hence we call a recovered weight vector $\hat{\omega}$ a *successful recovery* of ω^* if $\hat{\omega} = c\omega^*$ with $c \neq 0$, and the specific $c > 0$ can be found by using normalization (Keshavarz et al., 2011).

We have noted that existing techniques for IOC typically assume that complete observations of the trajectory of states and inputs ($\mathbf{x}_{1:T}^*, \mathbf{u}_{1:T}^*$) are available. Violation of this will lead to a failure of existing approaches. In this article, we aim to develop a methodology for using incomplete observations to solve the IOC problem. Provided a relevant feature set \mathcal{F}^* , our goal is to achieve a successful recovery of ω^* to $\text{col } \mathcal{F}^*$ based on incomplete observations of the trajectory of states and inputs ($\mathbf{x}_{t:t+l-1}^*, \mathbf{u}_{t:t+l-1}^*$) with $1 \leq t \leq t+l-1 \leq T$. Here, t is called the *observation starting time* and l called the *observation length*. Furthermore, we want to find minimal observations of the trajectory, i.e. the minimal length l_{\min} , which suffices for this purpose.

III. THE RECOVERY MATRIX FOR IOC

In this section, we propose the concept of the *recovery matrix* and demonstrate its relationship to solving IOC problems. Properties associated with the recovery matrix provide insights for the IOC process in terms of trajectory observations and feature selection. Algorithms for computing the recovery matrix and its properties are also presented. The recovery matrix as well as its properties will serve as a foundation for developing the approaches to address IOC with incomplete observations.

A. Definition of the Recovery Matrix

In the following, we first present the formal definition of the recovery matrix, then establish its relation with cost function recovery, which is also the motivation of the recovery matrix.

Definition 1. Given observations of the trajectory of states and inputs ($\mathbf{x}_{t:t+l-1}^*, \mathbf{u}_{t:t+l-1}^*$) for the system (1) with $1 \leq t \leq t+l-1 \leq T$, and an arbitrary feature set $\mathcal{F} = \{\phi_1, \phi_2, \dots, \phi_r\}$. Let $\phi = \text{col } \mathcal{F}$. Then the recovery matrix, denoted by $\mathbf{H}(t, l)$, is defined as

$$\mathbf{H}(t, l) = [\mathbf{H}_1(t, l) \quad -\mathbf{H}_2(t, l)] \in \mathbb{R}^{ml \times (r+n)} \quad (4)$$

with

$$\mathbf{H}_1(t, l) = \mathbf{F}_u(t, l)\mathbf{F}_x^{-1}(t, l)\Phi_x(t, l) + \Phi_u(t, l) \quad (5)$$

$$\mathbf{H}_2(t, l) = \mathbf{F}_u(t, l)\mathbf{F}_x^{-1}(t, l)\mathbf{V}(t, l). \quad (6)$$

Here, $\mathbf{F}_x(t, l)$, $\mathbf{F}_u(t, l)$, $\Phi_x(t, l)$, $\Phi_u(t, l)$ and $\mathbf{V}(t, l)$ are respectively defined as follows:

$$\mathbf{F}_x(t, l) = \begin{bmatrix} I & -\frac{\partial \mathbf{f}'}{\partial \mathbf{x}_t^*} & & \\ & I & \ddots & \\ & & \ddots & -\frac{\partial \mathbf{f}'}{\partial \mathbf{x}_{t+l-2}^*} \\ & & & I \end{bmatrix} \in \mathbb{R}^{nl \times nl}; \quad (7)$$

$$\mathbf{F}_u(t, l) = \begin{bmatrix} \frac{\partial \mathbf{f}'}{\partial \mathbf{u}_t^*} & & & \\ & \frac{\partial \mathbf{f}'}{\partial \mathbf{u}_{t+1}^*} & & \\ & & \ddots & \\ & & & \frac{\partial \mathbf{f}'}{\partial \mathbf{u}_{t+l-1}^*} \end{bmatrix} \in \mathbb{R}^{ml \times nl}; \quad (8)$$

$$\Phi_x(t, l) = \begin{bmatrix} \frac{\partial \phi}{\partial \mathbf{x}_t^*} & \frac{\partial \phi}{\partial \mathbf{x}_{t+1}^*} & \dots & \frac{\partial \phi}{\partial \mathbf{x}_{t+l-1}^*} \end{bmatrix}' \in \mathbb{R}^{nl \times r}; \quad (9)$$

$$\Phi_u(t, l) = \begin{bmatrix} \frac{\partial \phi}{\partial \mathbf{u}_t^*} & \frac{\partial \phi}{\partial \mathbf{u}_{t+1}^*} & \dots & \frac{\partial \phi}{\partial \mathbf{u}_{t+l-1}^*} \end{bmatrix}' \in \mathbb{R}^{ml \times r}; \quad (10)$$

$$\mathbf{V}(t, l) = \begin{bmatrix} \mathbf{0} & \frac{\partial \mathbf{f}}{\partial \mathbf{x}_{t+l-1}^*} \end{bmatrix}' \in \mathbb{R}^{nl \times n} \quad (11)$$

with $\frac{\partial \mathbf{f}}{\partial \mathbf{x}_T^*} = I$.

In order to show the relation between the recovery matrix defined above and cost function recovery, we next establish the following assumption for the given feature set.

Assumption 1. The feature set \mathcal{F} in Definition 1 contains a subset of relevant features \mathcal{F}^* , i.e. $\mathcal{F}^* \subseteq \mathcal{F}$.

Assumption 1 requires that the given feature set contains a subset of relevant features that can be used to characterize the optimal trajectory as in (2), and also allows for additional features that are irrelevant to express the trajectory. Although restrictive for the choice of features, the assumption is likely to be fulfilled in practice by providing a larger set including many features when exact feature knowledge is not available.

Under Assumption 1, without loss of generality, consider

$$\mathcal{F} = \{\phi_1^*, \phi_2^*, \dots, \phi_s^*, \bar{\phi}_{s+1}, \dots, \bar{\phi}_r\} \quad (12)$$

where the first s elements are from \mathcal{F}^* (3). Then we have

$$\phi(\mathbf{x}, \mathbf{u}) = \text{col } \mathcal{F} = \begin{bmatrix} \phi^*(\mathbf{x}, \mathbf{u}) \\ \bar{\phi}(\mathbf{x}, \mathbf{u}) \end{bmatrix} \in \mathbb{R}^r \quad (13)$$

where $\phi^* \in \mathbb{R}^s$ is the relevant feature vector (2) while vector $\bar{\phi} \in \mathbb{R}^{(r-s)}$ corresponds to the irrelevant features that are not in \mathcal{F}^* . We define a weight vector corresponding to (13) as

$$\omega = [\omega_1^* \quad \omega_2^* \quad \dots \quad \omega_s^* \quad 0 \quad \dots \quad 0] \in \mathbb{R}^r. \quad (14)$$

Here, the first s entries are the feature weights corresponding to the relevant features in \mathcal{F}^* and the other feature weights are zeros. Then according to (2), we can say that the optimal trajectory ($\mathbf{x}_{1:T}^*, \mathbf{u}_{1:T}^*$) (locally) minimizes

$$J(\mathbf{x}_{1:T}, \mathbf{u}_{1:T}) = \sum_{k=1}^T \omega' \phi(\mathbf{x}_k, \mathbf{u}_k). \quad (15)$$

We now consider the optimal control problem in (15) with the system dynamics in (1). The resultant optimal trajectory

is governed by the KKT optimality criteria with the following Lagrange function

$$L = J(\mathbf{x}_{1:T}, \mathbf{u}_{1:T}) + \sum_{k=1}^T \boldsymbol{\lambda}'_k (\mathbf{x}_k - \mathbf{f}(\mathbf{x}_{k-1}, \mathbf{u}_k)) \quad (16)$$

where $\boldsymbol{\lambda}_k \in \mathbb{R}^n$ is the costate variable (Lagrange multiplier) for $1 \leq k \leq T$. The optimal solution is given by

$$\frac{\partial L}{\partial \mathbf{x}_{1:T}^*} = \mathbf{0} \quad (17a)$$

$$\frac{\partial L}{\partial \mathbf{u}_{1:T}^*} = \mathbf{0}. \quad (17b)$$

Based on (7)-(11), (17a) and (17b) can be represented by

$$\mathbf{F}_x(1, T) \boldsymbol{\lambda}_{1:T} + \Phi_x(1, T) \boldsymbol{\omega} = \mathbf{0} \quad (18a)$$

$$-\mathbf{F}_u(1, T) \boldsymbol{\lambda}_{1:T} + \Phi_u(1, T) \boldsymbol{\omega} = \mathbf{0}, \quad (18b)$$

respectively, with $\boldsymbol{\lambda}_{1:T} = \text{col} \{\boldsymbol{\lambda}_1, \boldsymbol{\lambda}_2, \dots, \boldsymbol{\lambda}_T\}$. Under complete observations of the trajectory, (18) forms the main idea for typical KKT-based IOC methods (e.g. Englert et al., 2017; Molloy et al., 2018; Puydupin-Jamin et al., 2012), where both the costates $\boldsymbol{\lambda}_{1:T}$ and $\boldsymbol{\omega}$ are estimated.

Given incomplete trajectory data $(\mathbf{x}_{t:t+l-1}^*, \mathbf{u}_{t:t+l-1}^*)$, the following equations can be established by partitioning (18a) and (18b) in rows as follows

$$\mathbf{F}_x(t, l) \boldsymbol{\lambda}_{t:t+l-1} + \Phi_x(t, l) \boldsymbol{\omega} = \boldsymbol{\epsilon}; \quad (19a)$$

$$-\mathbf{F}_u(t, l) \boldsymbol{\lambda}_{t:t+l-1} + \Phi_u(t, l) \boldsymbol{\omega} = \mathbf{0}, \quad (19b)$$

where

$$\boldsymbol{\epsilon} = \mathbf{V}(t, l) \boldsymbol{\lambda}_{t+l} = \begin{bmatrix} \mathbf{0} \\ \frac{\partial \mathbf{f}'}{\partial \mathbf{x}_{t+l}^*} \boldsymbol{\lambda}_{t+l} \end{bmatrix} \in \mathbb{R}^{nl},$$

with $1 \leq t \leq t+l-1 \leq T$. Note that when $t+l-1 = T$, since $\frac{\partial \mathbf{f}}{\partial \mathbf{x}_T^*}$ and $\boldsymbol{\lambda}_{T+1}$ are not defined, we here particularly let $\frac{\partial \mathbf{f}}{\partial \mathbf{x}_T^*} = \mathbf{I}$ and $\boldsymbol{\lambda}_{T+1} = \mathbf{0}$.

By noticing the fact that $\mathbf{F}_x(t, l)$ is always invertible, we combine (19a) with (19b) and cancel out $\boldsymbol{\lambda}_{t:t+l-1}$, leading to

$$\begin{aligned} & \left((\mathbf{F}_u(t, l) \mathbf{F}_x^{-1}(t, l) \Phi_x(t, l) + \Phi_u(t, l)) \boldsymbol{\omega} \right. \\ & \left. - (\mathbf{F}_u(t, l) \mathbf{F}_x^{-1}(t, l) \mathbf{V}(t, l)) \boldsymbol{\lambda}_{t+l} \right) = \mathbf{0}. \end{aligned} \quad (20)$$

Considering the definition of the recovery matrix in (5)-(6), (20) can be written as

$$\mathbf{H}_1(t, l) \boldsymbol{\omega} - \mathbf{H}_2(t, l) \boldsymbol{\lambda}_{t+l} = \mathbf{H}(t, l) \begin{bmatrix} \boldsymbol{\omega} \\ \boldsymbol{\lambda}_{t+l} \end{bmatrix} = \mathbf{0}. \quad (21)$$

Equations (20) and (21) reveal that the weight vector $\boldsymbol{\omega}$ and costate $\boldsymbol{\lambda}_{t+l}$ form the solution to a linear equation, where the coefficient matrix, namely the recovery matrix, is determined by the available trajectory observations $(\mathbf{x}_{t:t+l-1}^*, \mathbf{u}_{t:t+l-1}^*)$ and the selected feature vector ϕ . Here, the unknown costate $\boldsymbol{\lambda}_{t+l}$ can be interpreted as a variable encoding information of the future trajectory beyond the current observation range, and when the observations reach the trajectory terminal, i.e. $t+l-1 = T$, $\boldsymbol{\lambda}_{T+1} = \mathbf{0}$ indicating no future information.

Therefore, recovery of the cost function from incomplete observations should also account for the future information beyond the current observations, i.e. the costate $\boldsymbol{\lambda}_{t+l}$ in (21). The following theorem establishes the relationship between the recovery matrix and recovering the weights of candidate features given incomplete observations of the trajectory.

Theorem 1. *Suppose that under Assumption 1, the recovery matrix $\mathbf{H}(t, l)$ is given in Definition 1. Let any $\text{col} \{\hat{\boldsymbol{\omega}}, \hat{\boldsymbol{\lambda}}\} \in \ker \mathbf{H}(t, l)$ with $\hat{\boldsymbol{\omega}} \in \mathbb{R}^r$. If*

$$\text{rank } \mathbf{H}(t, l) = r + n - 1 \quad \text{and} \quad \text{col} \{\hat{\boldsymbol{\omega}}, \hat{\boldsymbol{\lambda}}\} \neq \mathbf{0}, \quad (22)$$

then there exists a constant $c \neq 0$ such that the i th entries in $\hat{\boldsymbol{\omega}}$ and ϕ satisfy

$$\hat{\omega}_i = \begin{cases} c\omega_i^*, & \text{if } \phi_i \in \mathcal{F}^* \\ 0, & \text{otherwise} \end{cases} \quad (23)$$

for $1 \leq i \leq r$, and vector $\text{col} \{\hat{\omega}_i \mid \phi_i \in \mathcal{F}^, 1 \leq i \leq r\} = c\boldsymbol{\omega}^*$, which is a successful recovery of $\boldsymbol{\omega}^*$.*

Proof. Given observations $(\mathbf{x}_{t:t+l-1}^*, \mathbf{u}_{t:t+l-1}^*)$ and feature set $\mathcal{F} \supset \mathcal{F}^*$, there exists $\boldsymbol{\lambda}_{t+l} \in \mathbb{R}^n$ such that (21) holds, i.e.

$$\mathbf{H}(t, l) \begin{bmatrix} \boldsymbol{\omega} \\ \boldsymbol{\lambda}_{t+l} \end{bmatrix} = \mathbf{0}, \quad (24)$$

with $\boldsymbol{\omega} \neq \mathbf{0}$ defined in (14). Since $\text{col} \{\hat{\boldsymbol{\omega}}, \hat{\boldsymbol{\lambda}}\} \in \ker \mathbf{H}(t, l)$ and the condition (22), it follows that the kernel of $\mathbf{H}(t, l)$ is one-dimensional and $\hat{\boldsymbol{\omega}} = c\boldsymbol{\omega}$ ($c \neq 0$). Therefore, we can conclude that $\hat{\boldsymbol{\omega}}$ is a scaled version of $\boldsymbol{\omega}$, and that the entries in $\hat{\boldsymbol{\omega}}$ corresponding to the relevant features in \mathcal{F}^* will stack a column vector which is a successful recovery of $\boldsymbol{\omega}^*$. This completes the proof. ■

Remark. *From Theorem 1, under Assumption 1 the rank of the recovery matrix provides a guarantee for whether one is able to recover the weights of the candidate features using incomplete observations of the trajectory. If so, the recovered weights can be found in the kernel of the recovery matrix: the weights corresponding to irrelevant features are zeros, and weights of relevant features form a weight vector which is a successful recovery for the IOC problem.*

B. Properties of the Recovery Matrix

Based on Definition 1, we explore the properties associated with the recovery matrix, which provides us a better understanding of how the information from the observations and selected features is incorporated into the recovery matrix. We first present an iterative formula for the recovery matrix.

Lemma 1 (Iterative Property). *For any $1 \leq t \leq t+l-1 < T$, one has*

$$\begin{aligned} \mathbf{H}(t, l+1) &= [\mathbf{H}_1(t, l+1) \quad -\mathbf{H}_2(t, l+1)] \quad (25) \\ &= \begin{bmatrix} \mathbf{H}_1(t, l) & -\mathbf{H}_2(t, l) \\ \frac{\partial \phi'}{\partial \mathbf{u}_{t+l}^*} & -\frac{\partial \mathbf{f}'}{\partial \mathbf{u}_{t+l}^*} \end{bmatrix} \begin{bmatrix} \mathbf{I} & \mathbf{0} \\ -\frac{\partial \phi'}{\partial \mathbf{x}_{t+l}^*} & \frac{\partial \mathbf{f}'}{\partial \mathbf{x}_{t+l}^*} \end{bmatrix} \end{aligned}$$

with initial $\mathbf{H}(t, 1)$ for a single observation $(\mathbf{x}_t^, \mathbf{u}_t^*)$*

$$\mathbf{H}(t, 1) = [\mathbf{H}_1(t, 1) \quad -\mathbf{H}_2(t, 1)]$$

$$= \left[\begin{array}{c} \left(\frac{\partial \mathbf{f}'}{\partial \mathbf{u}_i^*} \frac{\partial \phi'}{\partial \mathbf{x}_i^*} + \frac{\partial \phi'}{\partial \mathbf{u}_i^*} \right) \\ - \frac{\partial \mathbf{f}'}{\partial \mathbf{u}_i^*} \frac{\partial \mathbf{f}'}{\partial \mathbf{x}_i^*} \end{array} \right] \quad (26)$$

Proof. Please see Appendix A. ■

The iterative property describes an efficient way to calculate the recovery matrix; that is, by recursively integrating each new observation into the current representation. This property will be employed for efficiently computing the IOC problem, as shown in Section IV.

As the recovery matrix is dependent upon the observations of the trajectory and selected features, in the following two lemmas, we will show how these two factors influence the recovery matrix and the recovery of cost functions.

For trajectory observations, we expect that more data may render the observations more informative to infer the cost function. This is described by the following lemma.

Lemma 2 (Rank Nondecreasing). *For any $1 \leq t \leq t+l-1 < T$ and any given feature set \mathcal{F} , one has*

$$\text{rank } \mathbf{H}(t, l) \leq \text{rank } \mathbf{H}(t, l+1) \quad (27)$$

if new observation $(\mathbf{x}_{t+l}^, \mathbf{u}_{t+l}^*)$ has $\det\left(\frac{\partial \mathbf{f}}{\partial \mathbf{x}_{t+l}^*}\right) \neq 0$.*

Proof. Please see Appendix B. ■

In Theorem 1, we have noted that the rank of the recovery matrix is related to whether one is able to recover the feature weights. Thus the rank of the recovery matrix can be viewed as an indicator for the richness of the current observations with respect to the provided feature set. Lemma 2 postulates that the richness of observations tends to increase when more trajectory data is integrated, and this increase is independent of choices of features.

The following lemma provides a necessary condition for the rank of the recovery matrix when given features contains a subset of features which can be used to characterize the observed trajectory as in (2).

Lemma 3 (Rank Upper Bound). *Suppose that Assumption 1 holds. Then for any $1 \leq t \leq t+l-1 \leq T$, the recovery matrix satisfies*

$$\text{rank } \mathbf{H}(t, l) \leq r + n - 1. \quad (28)$$

If there exists another subset of relevant features $\tilde{\mathcal{F}} \subseteq \mathcal{F}$ with corresponding weight vector $\tilde{\omega}$ under which the trajectory $(\mathbf{x}_{1:T}^, \mathbf{u}_{1:T}^*)$ are optimal, here $\tilde{\mathcal{F}} \neq \mathcal{F}^*$ or $\tilde{\omega} \neq \omega^*$, then the inequality (28) strictly holds, i.e.*

$$\text{rank } \mathbf{H}(t, l) < r + n - 1. \quad (29)$$

Proof. Please see Appendix C. ■

Lemma 3 states that if the provided feature set contains a subset of relevant features which can be used to characterize the optimal trajectory, the kernel of the recovery matrix is at least one-dimensional. Particularly when there exist more than one combination of relevant features in the provided feature set, which means different subsets of relevant features or different (or independent) corresponding weight vectors, then (22) in Theorem 1 is *impossible* to be fulfilled regardless

of the observation length and time. Therefore, (29) implies that though Assumption 1 is likely to be satisfied by adopting a larger feature set which covers all possible features, it may also lead to the non-uniqueness of relevant features.

On the other hand, if Assumption 1 fails to hold, e.g., the given feature set \mathcal{F} is small and does not contain a *complete subset* of relevant features, then due to Lemma 2 the recovery matrix is more likely to have $\text{rank } \mathbf{H}(t, l) = r + n$ after a certain observation length. Thus, Lemma 3 can be leveraged to investigate whether the selection of candidate features is proper or not in practice.

Combining Lemma 2 and Lemma 3, one is able to show: under Assumption 1, (i) if the rank of the recovery matrix is less than $r + n - 1$, indicating that the current observations are not sufficient to infer the cost function, then increasing the observation length may increase the rank; and (ii) once the observations have $\text{rank } \mathbf{H}(t, l) = r + n - 1$, additional observations will not contribute to increasing the rank of the recovery matrix. As demonstrated in Section IV, this property will help us to find minimal observations which suffice for recovering the cost function.

C. Implementation of Rank Examination

In practice, directly checking rank of the recovery matrix is challenging due to the following reasons: (i) data noise in the observed trajectory; (ii) near-optimality of demonstrations, namely, the observed trajectory slightly deviates from the optimal trajectory; and (iii) computational rounding error. For robustness of implementation, we employ the following strategies to examine the rank of the recovery matrix.

1) *Normalization*: In the case when the observed trajectory is of low magnitude, the recovery matrix may have entries of magnitude rather close to zeros, which will affect checking of the matrix rank because of computing rounding error. Hence a normalization to the recovery matrix is performed before verifying its rank. Here we adopt

$$\bar{\mathbf{H}}(t, l) = \frac{\mathbf{H}(t, l)}{\|\mathbf{H}(t, l)\|_F}, \quad (30)$$

where $\|\cdot\|_F$ is the Frobenius norm, and we only consider the recovery matrix that is not zero matrix. Then

$$\text{rank } \bar{\mathbf{H}}(t, l) = \text{rank } \mathbf{H}(t, l) \quad (31)$$

2) *Rank Index*: We are only interested in whether the rank of the recovery matrix satisfies the rank condition in (22) of Theorem 1. Instead of directly investigating the rank, we choose to examine the singular values of $\bar{\mathbf{H}}(t, l)$ in (30) by introducing the following rank index

$$\kappa(t, l) = \frac{\sigma_2(\bar{\mathbf{H}}(t, l))}{\sigma_1(\bar{\mathbf{H}}(t, l))}. \quad (32)$$

Therefore, the rank condition of the recovery matrix for (22) is examined by the following rule

$$\kappa(t, l) \geq \gamma \quad \text{and} \quad l > \frac{r+n}{m}. \quad (33)$$

Here γ is a pre-defined threshold and ideally $\gamma = \infty$. As discussed in Section V, we will show how to choose γ .

IV. IOC FROM INCOMPLETE OBSERVATIONS

In this section, based on the recovery matrix, we address the IOC problem given incomplete observations of the optimal trajectory. Particularly, we aim to find minimal observations of the trajectory which suffice for this goal. We proceed by first presenting the methodology and then developing the implementation.

A. Methodology

The following theorem establishes a sufficient condition for recovering the weights of specified features from incomplete observations of the optimal trajectory.

Corollary 1.1 (IOC with Incomplete Observations). *Consider the incomplete observations of states and inputs of the system (1) $(\mathbf{x}_{t:t+l-1}^*, \mathbf{u}_{t:t+l-1}^*)$ with $1 \leq t \leq t+l-1 \leq T$ and the relevant feature set \mathcal{F}^* (3). Suppose that the recovery matrix $\mathbf{H}(t, l)$ is defined in Definition 1 with $\mathcal{F} = \mathcal{F}^*$. Let any col $\{\hat{\omega}, \hat{\lambda}\} \in \ker \mathbf{H}(t, l)$ and col $\{\hat{\omega}, \hat{\lambda}\} \neq \mathbf{0}$ with $\hat{\omega} \in \mathbb{R}^s$. If*

$$\text{rank } \mathbf{H}(t, l) = s + n - 1, \quad (34)$$

then $\hat{\omega}$ is a successful recovery of ω^* , i.e. there must exist a non-zero constant c such that $\hat{\omega} = c\omega^*$.

Proof. Since Corollary 1.1 is a special case of Theorem 1, following a similar procedure as in proof of Theorem 1, we can show that there must exist costates $\lambda_{1:T}^*$ such that the following KKT conditions hold:

$$\mathbf{F}_x(1, T)\lambda_{1:T}^* + \Phi_x^*(1, T)\omega^* = \mathbf{0} \quad (35a)$$

$$-\mathbf{F}_u(1, T)\lambda_{1:T}^* + \Phi_u^*(1, T)\omega^* = \mathbf{0} \quad (35b)$$

where $\Phi_x^*(1, T)$ and $\Phi_u^*(1, T)$ are respectively defined in (9) and (10), but with the relevant feature vector $\phi^* = \text{col } \mathcal{F}^*$ in place of ϕ . We can also establish the equations corresponding to the observations $(\mathbf{x}_{t:t+l-1}^*, \mathbf{u}_{t:t+l-1}^*)$:

$$\mathbf{F}_x(t, l)\lambda_{t:t+l-1}^* + \Phi_x^*(t, l)\omega^* = \mathbf{V}(t, l)\lambda_{t+l}^* \quad (36a)$$

$$-\mathbf{F}_u(t, l)\lambda_{t:t+l-1}^* + \Phi_u^*(t, l)\omega^* = \mathbf{0}, \quad (36b)$$

where $1 \leq t \leq t+l-1 \leq T$ and $\lambda_{T+1}^* = \mathbf{0}$. Combining (36a)-(36b) and eliminating $\lambda_{t:t+l-1}^*$ leads to

$$\begin{aligned} & \left((\mathbf{F}_u(t, l)\mathbf{F}_x^{-1}(t, l)\Phi_x^*(t, l) + \Phi_u^*(t, l))\omega^* \right. \\ & \left. - (\mathbf{F}_u(t, l)\mathbf{F}_x(t, l)\mathbf{V}(t, l))\lambda_{t+l}^* \right) = \mathbf{0}. \end{aligned} \quad (37)$$

Therefore, it follows that

$$\mathbf{H}(t, l) \begin{bmatrix} \omega^* \\ \lambda_{t+l}^* \end{bmatrix} = \mathbf{0}. \quad (38)$$

Since non-zero vector col $\{\hat{\omega}, \hat{\lambda}\} \in \ker \mathbf{H}(t, l)$ and the rank condition (34), it follows that the nullity of $\mathbf{H}(t, l)$ is one, and there must exist a constant $c \neq 0$ such that $\hat{\omega} = c\omega^*$. Thus $\hat{\omega}$ is a successful recovery of ω^* , which completes the proof. ■

Remark. *Compared to the KKT-based methods (e.g. Englert et al., 2017; Molloy et al., 2018; Puydupin-Jamin et al., 2012),*

where the main idea is to estimate col $\{\omega, \lambda_{1:T}\} \in \mathbb{R}^{s+Tn}$ directly via (35), Corollary 1.1 motivates a way to estimate col $\{\omega, \lambda\} \in \mathbb{R}^{s+n}$, which can be achieved from incomplete observations of length much smaller than T , due to the rank non-decreasing property of the recovery matrix (Lemma 2). We will show this advantage in Section V.

Remark. *If (34) in Corollary 1.1 is not satisfied, the rank of $\mathbf{H}(t, l)$ has to be less than $s + n - 1$ due to Lemma 3. We may find another weight vector independent of ω^* in the kernel of $\mathbf{H}(t, l)$. Thus, the current observations may result from weight vectors different than $c\omega^*$, indicating that the feature weights are not distinguishable with respect to the current observations. The reason may be due to insufficient observations or low data richness, which may be remedied by additional observations (see Lemma 2).*

B. Proposed Approach and Implementation

Combining Theorem 1 and properties of the recovery matrix, we have the following conclusions: (i) according to Lemma 2 more observations may contribute to the recovery matrix for satisfying (22), thus implying that the minimal observations, i.e. minimal observation length l_{\min} , sufficing for recovery can be found; (ii) according to Lemma 2 and lemma 3, the minimal observation length can also be found even if additional irrelevant features exist in the given feature set, and (iii) IOC with minimal observations can be efficiently performed. Therefore, we have the following approach.

Corollary 1.2 (Minimal Observation IOC). *Consider observation of the states and inputs of the system (1) from time t ($1 \leq t < T$) and a feature set \mathcal{F} under Assumption 1. The recovery matrix $\mathbf{H}(t, l)$, defined in (4)-(6) with \mathcal{F} , is updated at each time step with new observation via Lemma 1. Then the minimal observation length to guarantee a successful recovery is*

$$l_{\min}(t) = \min \{l \mid \text{rank } \mathbf{H}(t, l) = |\mathcal{F}| + n - 1\}, \quad (39)$$

and any col $\{\hat{\omega}, \hat{\lambda}\} \in \ker \mathbf{H}(t, l_{\min}(t))$ with col $\{\hat{\omega}, \hat{\lambda}\} \neq \mathbf{0}$ and $\hat{\omega} \in \mathbb{R}^{|\mathcal{F}|}$ has $\hat{\omega} = c\omega^*$ ($c \neq 0$), where $|\cdot|$ denotes the cardinality of a set, and ω^* is the weight vector of ground truth to col \mathcal{F} with the weights of irrelevant features zeros.

Proof. Corollary 1.2 is a direct application of Theorem 1, Lemma 1, Lemma 2 and Lemma 3. ■

Note that the minimal observation length stated above is the one that satisfies the rank condition as in (22). Obviously, l_{\min} varies subject to the observation starting time, trajectory data and selected features. A uniform lower bound, denoted as l_{\min}^* , to the minimal observation length can be found using the matrix rank property, which is

$$l_{\min}^* = \left\lceil \frac{(|\mathcal{F}| + n - 1)}{m} \right\rceil, \quad (40)$$

where $\lceil \cdot \rceil$ is the ceiling operator. Indeed, the observations of length l_{\min}^* are adequate for recovery if the trajectory data is informative enough. (40) also shows that adding additional

irrelevant features to the feature set affect the IOC procedure by increasing the minimal observations required for inferring the cost function.

In practical settings, directly applying Corollary 1.2 will be likely to fail in the presence of data noise, near-optimality of trajectory and computing error. Thus we use the following strategies for implementation. First, (39) can be investigated using the rank index in (32) as performed in (33). Second, computation of the successful recovery can be transformed into solving the following convex optimization

$$\begin{bmatrix} \hat{\omega} \\ \hat{\lambda} \end{bmatrix} = \arg \min \left\| \bar{\mathbf{H}}(t, l_{\min}(t)) \begin{bmatrix} \omega \\ \lambda \end{bmatrix} \right\|, \quad (41)$$

where $\|\cdot\|$ is the l_2 norm operator, and $\bar{\mathbf{H}}$ is the normalized recovery matrix (see (30)). Here, to avoid trivial solutions, we add the following constraint to the above optimization:

$$\sum_{i=1}^{|\mathcal{F}|} \omega_i = 1. \quad (42)$$

Finally, we present the overall realization of Corollary 1.2 in Algorithm 1.

Algorithm 1: Minimal Observation IOC Algorithm

Data: incomplete trajectory data from time t ;
feature set \mathcal{F} .

Output: successful recovery $\hat{\omega}$ of weight vector
corresponding to col \mathcal{F} .

Initial: initial observation length $l = 1$;
initial recovery matrix $\mathbf{H}(t, 1)$ (26);
normalization $\bar{\mathbf{H}}(t, 1)$ (30);
rank index threshold γ (33).

while (not satisfying (33)) **do**

extend observation length: $l = l + 1$;
take the next observation $(\mathbf{x}_{t+l}^*, \mathbf{u}_{t+l}^*)$;
update $\mathbf{H}(t, l)$ (25);
obtain $\bar{\mathbf{H}}(t, l)$ (30);

end

minimal observation length $l_{\min}(t) = l$ (39);
compute a successful recovery $\hat{\omega}$ via (41).

V. SIMULATIONS

The evaluation consists of two parts: first, we compare the performance of KKT-based methods (e.g. Englert et al., 2017; Molloy et al., 2018; Puydupin-Jamin et al., 2012) with ours; and second, on a simulated two-link robot arm, we evaluate the proposed minimal observation IOC algorithm in the presence of observation noise, irrelevant features, and parameter settings.

In order to quantify recovery accuracy of IOC, we define the following recovery error for the weight vector

$$e_\omega = \inf_{c>0} \frac{\|c\hat{\omega} - \omega^*\|}{\|\omega^*\|} \quad (43)$$

where $\|\cdot\|$ denotes the l_2 norm, $\hat{\omega}$ is the recovered weight vector, and ω^* is the ground truth value.

A. Comparison with KKT-Based Methods

We choose the inverse LQR problem to facilitate our analysis and demonstration. Consider a linear system

$$\mathbf{x}_{k+1} = \begin{bmatrix} -1 & 1 \\ 0 & 1 \end{bmatrix} \mathbf{x}_k + \begin{bmatrix} 1 \\ 3 \end{bmatrix} \mathbf{u}_{k+1} \quad (44)$$

with initial condition $\mathbf{x}_0 = [2, -2]'$ and time horizon $T = 100$. The quadratic cost function to be minimized is

$$J = \sum_{k=1}^T \mathbf{x}'_k Q \mathbf{x}_k + \sum_{k=1}^T \mathbf{u}'_k R \mathbf{u}_k \quad (45)$$

where Q and R are positive definite and are assumed to have the following structures:

$$Q = \begin{bmatrix} q_1^* & 0 \\ 0 & q_2^* \end{bmatrix}, \quad R = r^*, \quad (46)$$

respectively. Written in feature-weight form as in (2), (45) corresponds to the feature vector $\phi^* = [x_{1,k}^2, x_{2,k}^2, u_k^2]'$ and weight vector $\omega^* = [q_1^*, q_2^*, r^*]'$. We here specify the weight vector $\omega^* = [0.507, 0.845, 0.169]'$, and the resulting optimal trajectory of states and inputs is plotted in Fig. 1a.

Provided the feature vector ϕ^* , we study the influence of incomplete observations on weight vector recovery by means of KKT-based methods (e.g. Englert et al., 2017; Molloy et al., 2018; Puydupin-Jamin et al., 2012) and the proposed approach, in terms of varying observation length and starting time. We fix the starting time of observation at time 1, 3, 6, 54 and 84, respectively (as labeled with red arrows in Fig. 1a), and for each starting time we examine the recovery error (43) for KKT-based methods and the proposed method with increasing end time of observation (equivalent to increasing the observation length). Note that for the proposed approach, we compute the weight vector by

$$\begin{bmatrix} \hat{\omega} \\ \hat{\lambda} \end{bmatrix} = \arg \min \left\| \bar{\mathbf{H}}(t, l) \begin{bmatrix} \omega \\ \lambda \end{bmatrix} \right\|, \quad (47)$$

instead of finding the minimal observation length. Here, $\|\cdot\|$ denotes l_2 norm, and to avoid trivial solutions, we constrain the weight vector in both methods to have $\sum_{i=1}^3 \hat{\omega}_i = 1$. The comparison results for the different cases are depicted in Fig. 1b-1f. We have the following comments.

Robustness: as illustrated by the blue lines in Fig. 1b-1d, KKT-based methods show high sensitivity to choices of observation starting position. The observations starting from time 1, 3, and 6 lead to significant differences in recovery convergence. This is because the trajectory in Fig. 1a in the first 10 steps is more informative than the rest but converges very quickly (see Fig. 1a); thus a small change in observation outset will have a huge influence on the loss of data richness, leading to a significant increase of the observation length to compensate for this ‘loss’ and to maintain necessary richness against the unknown future information (as shown in (36), the future information is encoded in λ_{t+l}^* which is unknown for KKT-based methods). For example, as illustrated in Fig. 1b

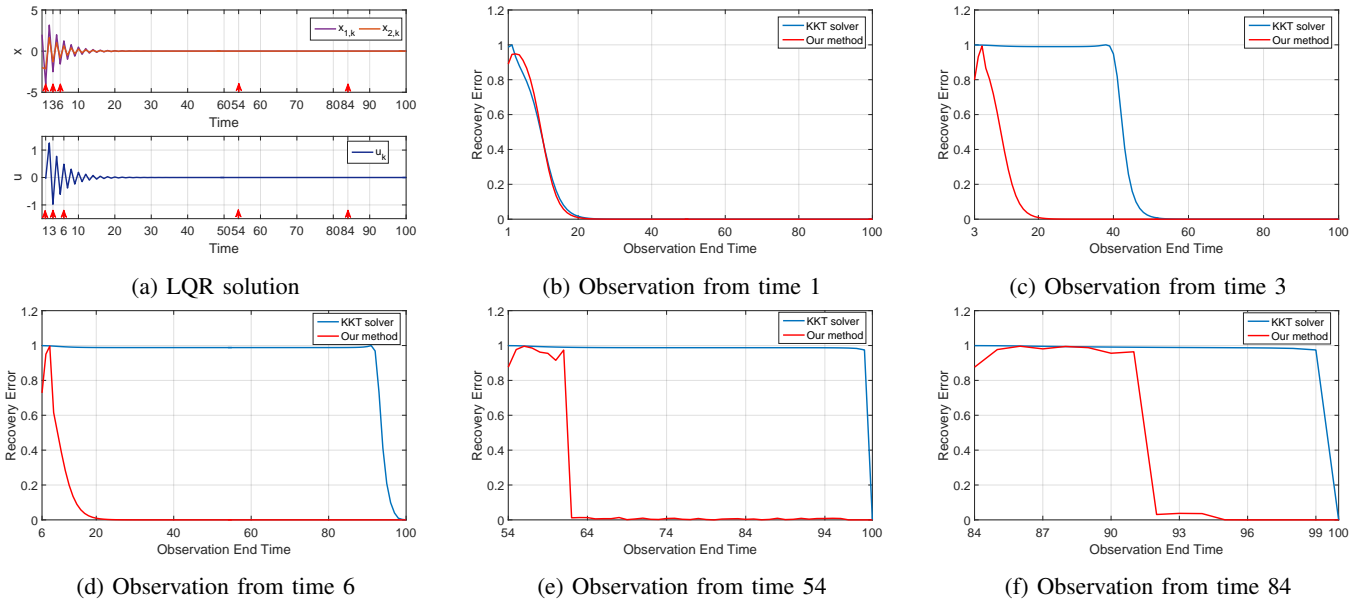


Figure 1: Influence of incomplete observations on recovery by KKT-based methods and the proposed method: Fig. 1a is the solution of LQR problem, where the red arrows are the labels of different observation starting times corresponding to the cases of Fig. 1b-1f, respectively; Fig. 1b-1f show the recovery error for KKT-based methods (blue lines) and our approach (red lines) when observation length increases.

and 1c, the change of observation starting time from 1 to 3 will lead to the increase of observation length from 25 to 60 to achieve correct convergence. By contrast, the performance of the proposed method (in red lines) is less sensitive to the choice of observation starting time, and always converges after around 20 steps. This advantage is because we include the future information in our formulation, as captured by the variable λ in (47).

Accuracy: for KKT-based methods, when the incomplete observations are less informative, the solutions are likely to converge to wrong values. For example, the observations in Fig. 1d-1f are less informative than those in Fig. 1b-1c, and thus until the observations reach the trajectory terminal, the solutions converge to $\hat{\omega} = [0.018, -0.382, 0.924]'$. This wrong convergence is due to two reasons: (i) KKT-based methods jointly optimizing the weights and costates of high dimensionality (see (35)) will likely have non-unique solutions; and (ii) as KKT-based methods only consider the current observations, future behavior beyond the observation window will have more significant influence especially when the current observations are less informative. By contrast, the proposed method always converges to successful recovery after the minimal observation length. Fig. 1e shows small fluctuations for our approach after convergence. This is because the trajectory with near-zero magnitude leads to rounding error in computing the recovery matrix, though we have adopted the normalization strategy (30).

To summarize, KKT-based methods cannot be guaranteed to correctly recover the cost function from incomplete observations. The proposed approach provides a systematic way to

confirm whether available observations are sufficient for cost function weight recovery and if so, to recover the weights from arbitrary starting and ending positions in observation sequence.

B. Optimal Control for a Two-link Robot Arm

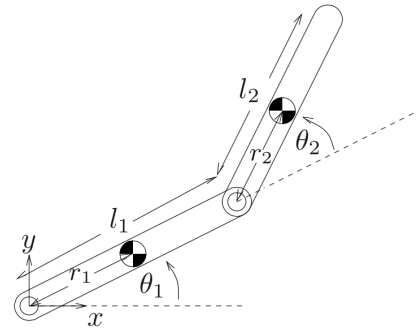


Figure 2: Two-link robot arm with coordinate definitions

To illustrate the proposed approach on a non-linear plant, we establish a model of a two-link robot arm which will be used for evaluating the proposed minimal observation IOC algorithm. Under the coordinates shown in Fig. 2, the inverse dynamics of a two-link arm moving in the vertical plane is

$$M(\theta)\ddot{\theta} + C(\theta, \dot{\theta})\dot{\theta} + g(\theta) = \tau, \quad (48)$$

where $\theta = [\theta_1, \theta_2]'$ is the joint angle vector; $M(\theta) \in \mathbb{R}^{2 \times 2}$ is the positive-definite inertia matrix; $C(\theta, \dot{\theta}) \in \mathbb{R}^{2 \times 2}$ is the Coriolis matrix; $g(\theta) \in \mathbb{R}^2$ is the gravity vector; and

$\boldsymbol{\tau} = [\tau_1, \tau_2]' \in \mathbb{R}^2$ are the torques applied to each joint. The above variables are explicitly defined as

$$\begin{aligned} M(\boldsymbol{\theta}) &= \begin{bmatrix} a_1 + 2a_2 \cos \theta_2 & a_3 + a_2 \cos \theta_2 \\ a_3 + a_2 \cos \theta_2 & a_3 \end{bmatrix} \\ C(\boldsymbol{\theta}, \dot{\boldsymbol{\theta}}) &= \begin{bmatrix} -a_2 \dot{\theta}_2 \sin \theta_2 & -a_2(\dot{\theta}_1 + \dot{\theta}_2) \sin \theta_2 \\ a_2 \dot{\theta}_1 \sin \theta_2 & 0 \end{bmatrix} \\ \mathbf{g}(\boldsymbol{\theta}) &= \begin{bmatrix} b_1 g \cos \theta_1 + b_2 g \cos(\theta_1 + \theta_2) \\ b_2 g \cos(\theta_1 + \theta_2) \end{bmatrix} \\ a_1 &= m_1 r_1^2 + m_2 (l_1^2 + r_2^2) + I_1 + I_2 \\ a_2 &= m_2 l_1 r_2 \\ a_3 &= m_2 r_2^2 + I_2 \\ b_1 &= l_1 m_2 + r_1 m_1 \\ b_2 &= r_2 m_2 \end{aligned}$$

where m_i is the mass of link i ($m_1 = 1\text{kg}$, $m_2 = 1\text{kg}$); l_i is the length of link i ($l_1 = 1\text{m}$, $l_2 = 1\text{m}$); r_i is the distance from the joint center to the center of mass for link i ($r_1 = 0.5\text{m}$, $r_2 = 0.5\text{m}$); and I_i is the moment of inertia with respect to the corresponding center of mass for link i ($I_1 = 0.5\text{kgm}^2$, $I_2 = 0.5\text{kgm}^2$).

From (48), the dynamics of the two-link robot arm is

$$\ddot{\boldsymbol{\theta}} = M(\boldsymbol{\theta})^{-1}(-C(\boldsymbol{\theta}, \dot{\boldsymbol{\theta}})\dot{\boldsymbol{\theta}} - \mathbf{g}(\boldsymbol{\theta}) + \boldsymbol{\tau}) \quad (49)$$

which can be further expressed in state-space representation

$$\dot{\mathbf{x}} = \mathbf{f}(\mathbf{x}, \mathbf{u}) \quad (50)$$

with the configuration state and torque input respectively given by

$$\mathbf{x} = [\theta_1 \quad \dot{\theta}_1 \quad \theta_2 \quad \dot{\theta}_2]', \text{ and } \mathbf{u} = \boldsymbol{\tau} = [\tau_1 \quad \tau_2]'. \quad (51)$$

In discrete-time settings, the optimal control problem for robot arm manipulation is formulated by

$$\begin{aligned} \min_{\mathbf{x}_{1:T}} \quad & \sum_{k=1}^T \boldsymbol{\omega}^* \boldsymbol{\phi}^*(x_k, u_k) \\ \text{s.t.} \quad & \mathbf{x}_{k+1} = \mathbf{x}_k + \Delta t \mathbf{f}(\mathbf{x}_k, \mathbf{u}_{k+1}) \\ & \mathbf{x}_0 = \mathbf{x}_{start} \\ & \mathbf{x}_T = \mathbf{x}_{goal}, \end{aligned} \quad (52)$$

where $\Delta t = 1/2000\text{s}$ is the discretization rate.

In (52), we specify the initial configuration of robot arm $\mathbf{x}_{start} = [0, 0, 0, 0]'$, final pose $\mathbf{x}_{goal} = [\pi/2, 0, -\pi/2, 0]'$, time horizon $T = 2000$, and the feature and weight vectors respectively

$$\boldsymbol{\phi}^* = [\tau_1^2 \quad \tau_2^2]' \text{ and } \boldsymbol{\omega}^* = [0.6 \quad 0.4]'. \quad (53)$$

We solve the optimal control problem in (52) by using Gpops Software (Patterson and Rao, 2014), and plot the resultant configuration trajectory in Fig. 3.

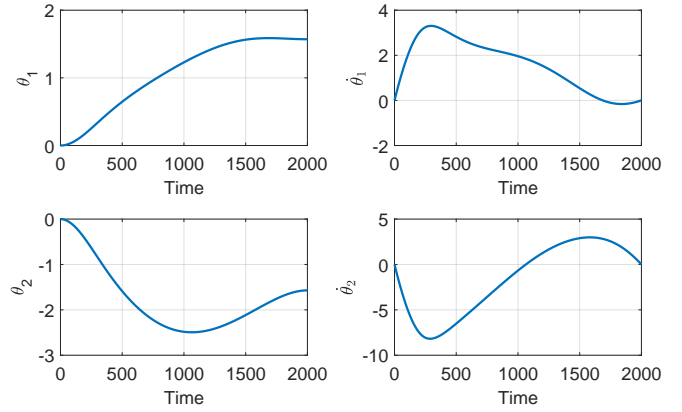


Figure 3: Configuration trajectory of a two-link robot arm

C. IOC from Incomplete Observations

Based on the configuration trajectory for the two-link robot arm in Fig. 3, we evaluate the proposed minimal observation IOC algorithm (Algorithm 1) in terms of data noise levels, presence of irrelevant features, and parameter settings, which are respectively presented below. Note that in each evaluation case, we process the configuration trajectory by (i) adding white Gaussian noise to simulate sensor noise and (ii) computing the torque (input) trajectory by (discretized) inverse dynamics in (48) to simulate real situations.

1) *Observation Noise*: we test the recovery performance of the proposed minimal observation IOC algorithm under different observation noise levels. Here we add to the trajectory data in Fig. 3 white Gaussian noise of different levels, which are characterized by the standard deviation $\sigma_1 = 1\text{e-}5$, $\sigma_2 = 1\text{e-}4$, and $\sigma_3 = 1\text{e-}3$, respectively.

To apply Algorithm 1, we provide the feature vector

$$\boldsymbol{\phi}^* = \begin{bmatrix} \phi_1^* \\ \phi_2^* \end{bmatrix} = \begin{bmatrix} \tau_1^2 \\ \tau_2^2 \end{bmatrix}, \quad (54)$$

and set $\gamma = 100$. We implement Algorithm 1 by beginning the observation at all time instants except for those near the trajectory terminal which do not provide the sufficient subsequent observation length to satisfy the minimal observation length requirements. The results of the algorithm for different noise levels are shown in Fig. 4.

In Fig. 4, the upper figures show the recovered weights based on minimal observations starting from varying times, and the bottom figures exhibit the corresponding minimal observation length. From the depicted results, our minimal observation IOC algorithm, regardless of observation starting time, generally demonstrates a stable and accurate performance while maintaining a low observation dimension. We summarize representative quantities of the plots in Table I to elaborate those advantages.

According to Table I, under fixed rank index threshold (here $\gamma = 100$), high noise levels will lead to larger average minimal observation length, but the average recovery error

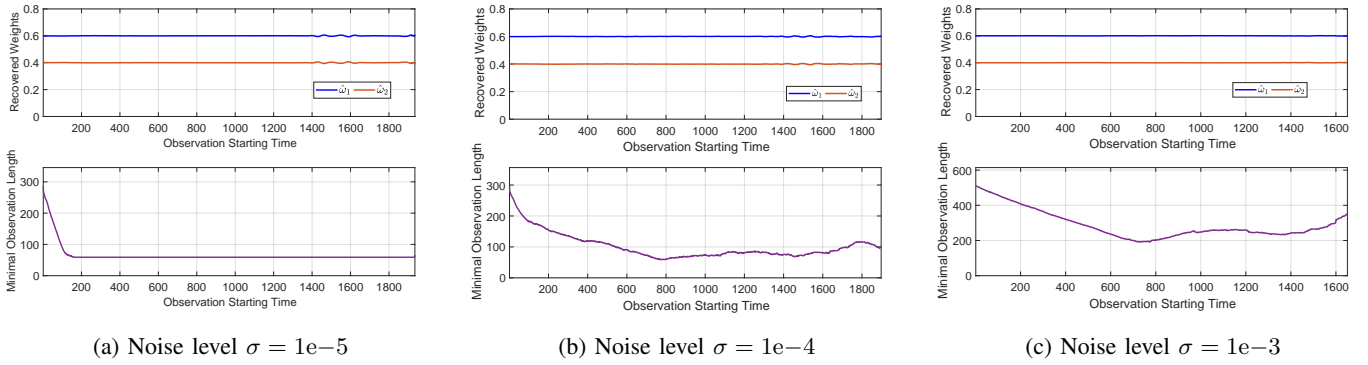


Figure 4: Recovery of weight vector for the motion of two-link robot arm under different observation noise levels; note that the weight vector of ground truth $[\omega_1^*, \omega_2^*]' = [0.6, 0.4]'$.

Table I: Results summary of feature weights recovery .

Noise level	Average $l_{\min}^{\dagger,1}$	Average recovery error e_{ω}^{\dagger}
$\sigma_1 = 1e-5$	65.40	0.0018
$\sigma_2 = 1e-4$	101.48	0.0017
$\sigma_3 = 1e-3$	288.90	0.0010

[†] For each noise level, the averaged values are computed by averaging all the corresponding quantities in Fig. 4 .

¹ Note that the overall time horizon $T = 2000$.

is not influenced too much. This is because the increased observation length compensates for the uncertainty induced by data noise and finally produces a ‘neutralized’ estimate. This thus proves the robustness of the proposed algorithm to observation noise.

2) *Presence of Irrelevant Features*: we here assume that exact knowledge of features is not available, and we evaluate the recovery performance of the proposed algorithm with an input feature set including irrelevant features. We use the trajectory in Fig. 3 with white Gaussian noise of standard deviation $\sigma = 1e-4$.

In Algorithm 1, we set $\gamma = 100$ and construct the input feature set from the following candidate features

$$\mathcal{F} = \{\tau_1^2, \tau_2^2, \tau_1^3, \tau_2^3, \tau_1^4, \tau_2^4\}. \quad (55)$$

The implementation of Algorithm 1 is the same as in the previous evaluations, that is, by beginning the recovery procedure at all time instants except for those near the trajectory terminal. We use the feature sets with different number of irrelevant features as listed in Table II, and for each case compute the average minimal observation length and recovery error. The results are summarized in Table II.

Table II shows that the average minimal observation length increases with additional irrelevant features added to the input feature set. This can be understood if we consider (39) and the rank non-decreasing property of the recovery matrix in Lemma 2: when a certain number of irrelevant features are included, the rank required for feature weight recovery will increase by the same amount, therefore requiring additional trajectory

Table II: Recovery under additional irrelevant features

Input feature set \mathcal{F}	Average l_{\min}^1	Average e_{ω}^2
$\{\tau_1^2, \tau_2^2\}$	101.48	0.0017
$\{\tau_1^2, \tau_2^2, \tau_1^3\}$	129.16	0.0017
$\{\tau_1^2, \tau_2^2, \tau_1^3, \tau_2^3\}$	243.79	0.0022
$\{\tau_1^2, \tau_2^2, \tau_1^3, \tau_2^3, \tau_1^4\}$	290.20	0.0026
$\{\tau_1^2, \tau_2^2, \tau_1^3, \tau_2^3, \tau_1^4, \tau_2^4\}$	413.82	0.0032

¹ Note that the overall time horizon $T = 2000$.

² The recovery error is computed via (43) and the weights of ground truth corresponding to irrelevant features are zeros.

observations. Because of the increased observation length, the accuracy of recovery is affected by the additional irrelevant features to a small extent (we will later show the accuracy can be improved by adjusting γ). Thus we conclude that the proposed algorithm is robust to the presence of irrelevant features.

3) *Parameter Setting*: we now discuss the choice of algorithm parameter, i.e. the rank index threshold γ , and its influence on recovery performance.

As performed in (32)-(33), γ is used to verify whether the rank of the recovery matrix satisfies (39) and determine the minimal observation length. Thus we first inspect how the value of γ affects the recovery performance of Algorithm 1. We use the trajectory data in Fig. 3 with white Gaussian noise added, with standard deviation $\sigma = 1e-4$, and provide the feature vector (54). The algorithm is implemented as done in previous evaluations, i.e. by starting the observation at all possible trajectory positions. We vary γ to show its influence on average minimal observation length and recovery error. The results are depicted in Fig. 5.

From Fig. 5, the value of γ influences the recovery process in the following aspects: (i) larger γ requires higher minimal observation length such that the data noise or other error sources, such as the error for discretizing dynamics, can be compensated by the increased observations; and (ii) because

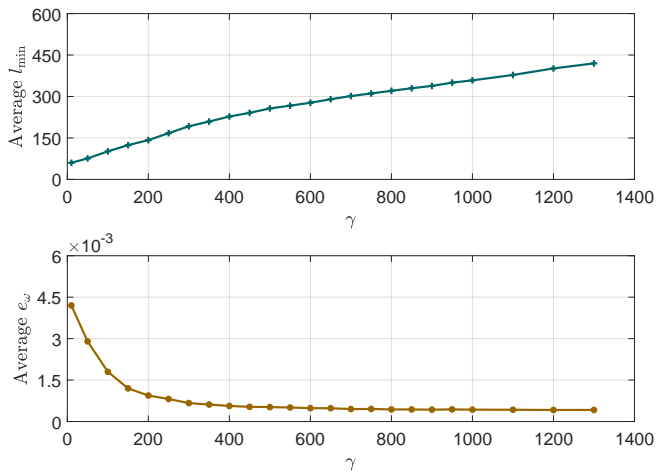


Figure 5: Influence of parameter γ on recovery

of the increased observation length, corresponding recovery accuracy is improved. However, as γ exceeds a certain value, such as 100 here, continuous increase of γ will not improve recovery accuracy significantly. This suggests that the choice of γ is not sensitive to recovery performance if the value is large. Therefore, in practice it is possible to find a proper γ without much manual effort such that both the recovery accuracy and computation costs are balanced. For example, in our case (noise level $\sigma = 1e - 4$), the suitable range for γ is [100, 600].

VI. CONCLUSIONS AND FUTURE WORK

We consider learning the cost function based on incomplete observations of an optimal trajectory. We handle the problem by proposing the recovery matrix, which establishes a relationship between any observations of the optimal trajectory and the unknown feature weights of given candidate features. The recovery matrix provides the following insights for addressing general inverse optimal control problems: first, additional observations of the trajectory may increase the rank of the recovery matrix, thus contributing to enabling the recovery; second, incomplete observations can be sufficient for inferring cost functions; third, the presence of irrelevant features does not influence recovery and can be identified; and fourth, IOC process can be solved in a more efficient way.

Built on the recovery matrix, a method for using incomplete observations of the optimal trajectory to recover the weights of specified features is established, and an algorithm of IOC based on minimal observations is developed. We apply the proposed approach to learn the cost function of a simulated two-link robot arm. The results demonstrate the stability, accuracy and robustness of the proposed method compared to the state of the art approaches. In the future, we will apply and extend the theory to the field of human-robot interaction.

ACKNOWLEDGMENTS

This research is partly supported by the ERC Starting Grant Control based on Human Models under grant agreement

337654 at Chair of Information-oriented Control, Technical University of Munich.

REFERENCES

- Pieter Abbeel and Andrew Y Ng. Apprenticeship learning via inverse reinforcement learning. In *Proceedings of the twenty-first international conference on Machine learning*, 2004.
- Pieter Abbeel, Adam Coates, and Andrew Y Ng. Autonomous helicopter aerobatics through apprenticeship learning. *The International Journal of Robotics Research*, 29(13):1608–1639, 2010.
- Navid Aghasadeghi and Timothy Bretl. Inverse optimal control for differentially flat systems with application to locomotion modeling. In *Proceedings of the IEEE International Conference on Robotics and Automation (ICRA)*, pages 6018–6025, 2014.
- Bastien Berret, Enrico Chiovetto, Francesco Nori, and Thierry Pozzo. Evidence for composite cost functions in arm movement planning: an inverse optimal control approach. *PLoS computational biology*, 7(10):e1002183, 2011.
- Sylvain Calinon, Florent D’halluin, Eric L Sauser, Darwin G Caldwell, and Aude G Billard. Learning and reproduction of gestures by imitation. *IEEE Robotics & Automation Magazine*, 17(2):44–54, 2010.
- Debora Clever, R Malin Schemschat, Martin L Felis, and Katja Mombaur. Inverse optimal control based identification of optimality criteria in whole-body human walking on level ground. In *Proceedings of the 6th IEEE International Conference on Biomedical Robotics and Biomechanics (BioRob)*, pages 1192–1199, 2016.
- Krishnamurthy Dvijotham and Emanuel Todorov. Inverse optimal control with linearly-solvable mdps. In *Proceedings of the 27th International Conference on Machine Learning (ICML)*, pages 335–342, 2010.
- Peter Englert, Ngo Anh Vien, and Marc Toussaint. Inverse kkt: Learning cost functions of manipulation tasks from demonstrations. *The International Journal of Robotics Research*, 36:1474–1488, 2017.
- Miles Johnson, Navid Aghasadeghi, and Timothy Bretl. Inverse optimal control for deterministic continuous-time nonlinear systems. In *Proceedings of the 52nd Annual Conference on Decision and Control (CDC)*, pages 2906–2913, 2013.
- Arezou Keshavarz, Yang Wang, and Stephen Boyd. Imputing a convex objective function. In *Proceedings of the IEEE International Symposium on Intelligent Control (ISIC)*, pages 613–619, 2011.
- J Zico Kolter, Pieter Abbeel, and Andrew Y Ng. Hierarchical apprenticeship learning with application to quadruped locomotion. In *Advances in Neural Information Processing Systems*, pages 769–776, 2008.
- Miroslav Krstic and Panagiotis Tsiotras. Inverse optimal stabilization of a rigid spacecraft. *IEEE Transactions on Automatic Control*, 44(5):1042–1049, 1999.

Markus Kuderer, Shilpa Gulati, and Wolfram Burgard. Learning driving styles for autonomous vehicles from demonstration. In *Proceedings of the IEEE International Conference on Robotics and Automation (ICRA)*, pages 2641–2646, 2015.

Sergey Levine and Vladlen Koltun. Continuous inverse optimal control with locally optimal examples. In *Proceedings of the 29th International Conference on Machine Learning*, 2012.

Jonathan Feng-Shun Lin, Vincent Bonnet, Adina M Panchea, Nacim Ramdani, Gentiane Venture, and Dana Kulić. Human motion segmentation using cost weights recovered from inverse optimal control. In *Proceedings of the IEEE-RAS 16th International Conference on Humanoid Robots (Humanoids)*, pages 1107–1113, 2016.

Jim Mainprice, Rafi Hayne, and Dmitry Berenson. Predicting human reaching motion in collaborative tasks using inverse optimal control and iterative re-planning. In *Proceedings of the IEEE International Conference on Robotics and Automation (ICRA)*, pages 885–892, 2015.

Jim Mainprice, Rafi Hayne, and Dmitry Berenson. Goal set inverse optimal control and iterative replanning for predicting human reaching motions in shared workspaces. *IEEE Transactions on Robotics*, 32(4):897–908, 2016.

Timothy L Molloy, Dorian Tsai, Jason J Ford, and Tristan Perez. Discrete-time inverse optimal control with partial-state information: A soft-optimality approach with constrained state estimation. In *Proceedings of the IEEE 55th Conference on Decision and Control (CDC)*, pages 1926–1932, 2016.

Timothy L Molloy, Jason J Ford, and Tristan Perez. Finite-horizon inverse optimal control for discrete-time nonlinear systems. *Automatica*, 87:442–446, 2018.

Katja Mombaur, Anh Truong, and Jean-Paul Laumond. From human to humanoid locomotion—an inverse optimal control approach. *Autonomous robots*, 28(3):369–383, 2010.

Andrew Y Ng and Stuart J Russell. Algorithms for inverse reinforcement learning. In *Proceedings of the international conference on machine learning*, pages 663–670, 2000.

Taesung Park and Sergey Levine. Inverse optimal control for humanoid locomotion. In *Robotics Science and Systems Workshop on Inverse Optimal Control and Robotic Learning from Demonstration*, 2013.

Michael A Patterson and Anil V Rao. Gpops-ii: A matlab software for solving multiple-phase optimal control problems using hp-adaptive gaussian quadrature collocation methods and sparse nonlinear programming. *ACM Transactions on Mathematical Software (TOMS)*, 41(1):1–37, 2014.

Anne-Sophie Puydupin-Jamin, Miles Johnson, and Timothy Bretl. A convex approach to inverse optimal control and its application to modeling human locomotion. In *Proceedings of the IEEE International Conference on Robotics and Automation (ICRA)*, pages 531–536, 2012.

Nathan D Ratliff, J Andrew Bagnell, and Martin A Zinkevich. Maximum margin planning. In *Proceedings of the 23rd international conference on Machine learning*, pages 729–

736. ACM, 2006.

Dizan Vasquez, Billy Okal, and Kai O Arras. Inverse reinforcement learning algorithms and features for robot navigation in crowds: an experimental comparison. In *Proceedings of the IEEE/RSJ International Conference on Intelligent Robots and Systems (IROS)*, pages 1341–1346, 2014.

Brian D Ziebart, Andrew L Maas, J Andrew Bagnell, and Anind K Dey. Maximum entropy inverse reinforcement learning. In *Proceedings of the AAAI conference on Artificial intelligence*, pages 1433–1438. Chicago, IL, USA, 2008.

Matt Zucker, Nathan Ratliff, Martin Stolle, Joel Chestnutt, J Andrew Bagnell, Christopher G Atkeson, and James Kuffner. Optimization and learning for rough terrain legged locomotion. *The International Journal of Robotics Research*, 30(2):175–191, 2011.

APPENDIX

A. Proof of Lemma 1

Consider the recovery matrix $\mathbf{H}(t, l)$ corresponding to the observations $(\mathbf{x}_{t:t+l-1}^*, \mathbf{u}_{t:t+l-1}^*)$ with $1 \leq t < t+l-1 < T$, i.e., from time t and of length l . When a new observation $(\mathbf{x}_{t+l}^*, \mathbf{u}_{t+l}^*)$ arrives, from Definition 1, the updated recovery matrix is defined as

$$\mathbf{H}_1(t, l+1) = \mathbf{F}_u(t, l+1)\mathbf{F}_x^{-1}(t, l+1) \mathbf{\Phi}_x(t, l+1) + \mathbf{\Phi}_u(t, l+1) \quad (56)$$

and

$$\mathbf{H}_2(t, l+1) = \mathbf{F}_u(t, l+1)\mathbf{F}_x^{-1}(t, l+1)\mathbf{V}(t, l+1), \quad (57)$$

where $\mathbf{F}_x(t, l+1)$, $\mathbf{F}_u(t, l+1)$, $\mathbf{\Phi}_x(t, l+1)$, $\mathbf{\Phi}_u(t, l+1)$, and $\mathbf{V}(t, l+1)$, respectively defined in (7)-(11), are updated as follows:

$$\mathbf{\Phi}_u(t, l+1) = \begin{bmatrix} \mathbf{\Phi}_u(t, l) \\ \frac{\partial \phi'}{\partial \mathbf{u}_{t+l}^*} \end{bmatrix}; \quad (58a)$$

$$\mathbf{\Phi}_x(t, l+1) = \begin{bmatrix} \mathbf{\Phi}_x(t, l) \\ \frac{\partial \phi'}{\partial \mathbf{x}_{t+l}^*} \end{bmatrix}; \quad (58b)$$

$$\mathbf{F}_u(t, l+1) = \begin{bmatrix} \mathbf{F}_u(t, l) & \mathbf{0} \\ \mathbf{0} & \frac{\partial \mathbf{f}'}{\partial \mathbf{u}_{t+l}^*} \end{bmatrix}; \quad (58c)$$

$$\begin{aligned} \mathbf{F}_x^{-1}(t, l+1) &= \begin{bmatrix} \mathbf{F}_x(t, l) & -\mathbf{V}(t, l) \\ \mathbf{0} & \mathbf{I} \end{bmatrix}^{-1} \\ &= \begin{bmatrix} \mathbf{F}_x^{-1}(t, l) & \mathbf{F}_x^{-1}(t, l)\mathbf{V}(t, l) \\ \mathbf{0} & \mathbf{I} \end{bmatrix}. \end{aligned} \quad (58d)$$

Here (58d) is computed based on the fact

$$\begin{bmatrix} \mathbf{A} & \mathbf{B} \\ \mathbf{C} & \mathbf{D} \end{bmatrix}^{-1} = \begin{bmatrix} \mathbf{A}^{-1} + \mathbf{A}^{-1}\mathbf{B}\mathbf{K}^{-1}\mathbf{C}\mathbf{A}^{-1} & -\mathbf{A}^{-1}\mathbf{B}\mathbf{K}^{-1} \\ -\mathbf{K}^{-1}\mathbf{C}\mathbf{A}^{-1} & \mathbf{K}^{-1} \end{bmatrix}$$

with $\mathbf{K} = \mathbf{D} - \mathbf{C}\mathbf{A}^{-1}\mathbf{B}$ the Schur complement of the block matrix with respect to \mathbf{A} .

When considering (58a)-(58d), we can obtain

$$\begin{aligned} \mathbf{H}_1(t, l+1) &= \mathbf{F}_u(t, l+1)\mathbf{F}_x^{-1}(t, l+1)\Phi_x(t, l+1) \\ &\quad + \Phi_u(t, l+1) \\ &= \begin{bmatrix} \mathbf{F}_u(t, l)\mathbf{F}_x^{-1}(t, l)\Phi_x(t, l) + \Phi_u(t, l) \\ \frac{\partial \mathbf{f}'}{\partial \mathbf{u}_{t+l}^*} \frac{\partial \phi'}{\partial \mathbf{x}_{t+l}^*} + \frac{\partial \phi'}{\partial \mathbf{u}_{t+l}^*} \end{bmatrix} \\ &\quad + \begin{bmatrix} \mathbf{F}_u(t, l)\mathbf{F}_x^{-1}(t, l)\mathbf{V}(t, l) \frac{\partial \phi'}{\partial \mathbf{x}_{t+l}^*} \\ \mathbf{0} \end{bmatrix}. \end{aligned} \quad (59)$$

Combined with (5)-(6), the above (59) becomes

$$\mathbf{H}_1(t, l+1) = \begin{bmatrix} \mathbf{H}_1(t, l) + \mathbf{H}_2(t, l) \frac{\partial \phi'}{\partial \mathbf{x}_{t+l}^*} \\ \frac{\partial \mathbf{f}'}{\partial \mathbf{u}_{t+l}^*} \frac{\partial \phi'}{\partial \mathbf{x}_{t+l}^*} + \frac{\partial \phi'}{\partial \mathbf{u}_{t+l}^*} \end{bmatrix}. \quad (60)$$

Also from (58a)-(58d), we have

$$\begin{aligned} \mathbf{H}_2(t, l+1) &= \mathbf{F}_u(t, l+1)\mathbf{F}_x^{-1}(t, l+1)\mathbf{V}(t, l+1) \\ &= \begin{bmatrix} \mathbf{F}_u(t, l)\mathbf{F}_x^{-1}(t, l)\mathbf{V}(t, l) \frac{\partial \mathbf{f}'}{\partial \mathbf{x}_{t+l}^*} \\ \frac{\partial \mathbf{f}'}{\partial \mathbf{u}_{t+l}^*} \frac{\partial \mathbf{f}'}{\partial \mathbf{x}_{t+l}^*} \end{bmatrix} \\ &= \begin{bmatrix} \mathbf{H}_2(t, l) \frac{\partial \mathbf{f}'}{\partial \mathbf{x}_{t+l}^*} \\ \frac{\partial \mathbf{f}'}{\partial \mathbf{u}_{t+l}^*} \frac{\partial \mathbf{f}'}{\partial \mathbf{x}_{t+l}^*} \end{bmatrix}. \end{aligned} \quad (61)$$

Finally joining (60) with (61) and writing them in the matrix form lead to (25).

When $l = 1$, i.e. only data $(\mathbf{x}_t^*, \mathbf{u}_t^*)$, based on (7)-(11), we have $\mathbf{F}_x(t, 1) = I$, $\mathbf{F}_u(t, 1) = \partial \mathbf{f}' / \partial \mathbf{u}_t^*$, $\Phi_x(t, 1) = \partial \phi' / \partial \mathbf{x}_t^*$, $\Phi_u(t, 1) = \partial \phi' / \partial \mathbf{u}_t^*$, and $\mathbf{V}(t, 1) = \partial \mathbf{f}' / \partial \mathbf{x}_t^*$. Therefore, considering the definition of recovery matrix (4)-(6), we obtain (26). This completes the proof. ■

B. Proof of Lemma 2

From Lemma 1, we have

$$\begin{aligned} &\text{rank } \mathbf{H}(t, l+1) \\ &= \text{rank} \begin{bmatrix} \mathbf{H}_1(t, l) & -\mathbf{H}_2(t, l) \\ \frac{\partial \phi'}{\partial \mathbf{u}_{t+l}^*} & -\frac{\partial \mathbf{f}'}{\partial \mathbf{u}_{t+l}^*} \end{bmatrix} \begin{bmatrix} I & \mathbf{0} \\ -\frac{\partial \phi'}{\partial \mathbf{x}_{t+l}^*} & \frac{\partial \mathbf{f}'}{\partial \mathbf{x}_{t+l}^*} \end{bmatrix}. \end{aligned} \quad (62)$$

If $\det(\frac{\partial \mathbf{f}'}{\partial \mathbf{x}_{t+l}^*}) \neq 0$, the last block matrix in (62) is non-singular. Consequently

$$\begin{aligned} \text{rank } \mathbf{H}(t, l+1) &= \text{rank} \begin{bmatrix} \mathbf{H}_1(t, l) & -\mathbf{H}_2(t, l) \\ \frac{\partial \phi'}{\partial \mathbf{u}_{t+l}^*} & -\frac{\partial \mathbf{f}'}{\partial \mathbf{u}_{t+l}^*} \end{bmatrix} \\ &\geq \text{rank} \begin{bmatrix} \mathbf{H}_1(t, l) & -\mathbf{H}_2(t, l) \end{bmatrix} \\ &= \text{rank } \mathbf{H}(t, l). \end{aligned} \quad (63)$$

Note that both (62) and the inequality (63) are independent of ϕ . This completes the proof. ■

C. Proof of Lemma 3

We first prove (28). Without loss of generality, we consider the feature set (12). Given observations $(\mathbf{x}_{t:t+l-1}^*, \mathbf{u}_{t:t+l-1}^*)$, then (21) holds, i.e.

$$\mathbf{H}(t, l) \begin{bmatrix} \boldsymbol{\omega} \\ \boldsymbol{\lambda}_{t+l} \end{bmatrix} = \mathbf{0}. \quad (64)$$

with $\boldsymbol{\omega} \neq \mathbf{0}$ defined in (14) and $\boldsymbol{\lambda}_{t+l}$ the costate at time step $t+l$. Note that (64) holds for any incomplete observations $(\mathbf{x}_{t:t+l-1}^*, \mathbf{u}_{t:t+l-1}^*)$ with $1 \leq t \leq t+l-1 \leq T$. Thus, the nullity of $\mathbf{H}(t, l)$ is at least one, which means

$$\text{rank } \mathbf{H}(t, l) \leq r + n - 1.$$

We then prove (29). When another relevant feature subset $\tilde{\mathcal{F}}$ exists in \mathcal{F} with associated weight vector $\tilde{\boldsymbol{\omega}}$, we can still construct a weight vector $\tilde{\boldsymbol{\omega}}$ corresponding to $\text{col } \mathcal{F}$ as in (14); that is, the weight entries in $\tilde{\boldsymbol{\omega}}$, which corresponds to features in $\tilde{\mathcal{F}}$ are from $\tilde{\boldsymbol{\omega}}$ and others zeros. Then following the similar derivations as from (15) to (21), we can obtain that there exists $\tilde{\boldsymbol{\lambda}}_{t+l} \in \mathbb{R}^n$ such that

$$\mathbf{H}(t, l) \begin{bmatrix} \tilde{\boldsymbol{\omega}} \\ \tilde{\boldsymbol{\lambda}}_{t+l} \end{bmatrix} = \mathbf{0}. \quad (65)$$

Since $\tilde{\mathcal{F}} \neq \mathcal{F}^*$ or $\tilde{\boldsymbol{\omega}} \neq \boldsymbol{\omega}^*$, then $\tilde{\boldsymbol{\omega}} \neq \boldsymbol{\omega}$. From (64) and (65), it follows that the nullity of $\mathbf{H}(t, l)$ is at least two, thus

$$\text{rank } \mathbf{H}(t, l) < r + n - 1.$$

This completes the proof. ■